Doubly Fed Induction Generator in an Offshore Wind Power Plant Operated at Rated V/Hz

Preprint

Eduard Muljadi, Mohit Singh,
and Vahan Gevorgian

To be presented at the IEEE Energy Conversion Congress and Exhibition
Raleigh, North Carolina
September 15-20, 2012

Conference Paper
NREL/CP-5500-55573
June 2012

Contract No. DE-AC36-08GO28308

Available electronically at http://www.osti.gov/bridge

Available for a processing fee to U.S. Department of Energy
and its contractors, in paper, from:

U.S. Department of Energy
Office of Scientific and Technical Information
P.O. Box 62
Oak Ridge, TN 37831-0062
phone: 865.576.8401
fax: 865.576.5728
email: mailto:reports@adonis.osti.gov

Available for sale to the public, in paper, from:

U.S. Department of Commerce
National Technical Information Service
5285 Port Royal Road
Springfield, VA 22161
phone: 800.553.6847
fax: 703.605.6900
email: orders@ntis.fedworld.gov
online ordering: http://www.ntis.gov/help/ordermethods.aspx

Cover Photos: (left to right) PIX 16416, PIX 17423, PIX 16560, PIX 17613, PIX 17436, PIX 17721

Printed on paper containing at least 50% wastepaper, including 10% post consumer waste.

Doubly Fed Induction Generator in an Offshore Wind Power Plant Operated at Rated V/Hz

E. Muljadi, *Fellow, IEEE*, M. Singh, *Member, IEEE*, and V. Gevorgian, *Member, IEEE*

***Abstract*—This paper introduces the concept of constant volt/hertz operation of offshore wind power plants (WPPs). The deployment of offshore WPPs requires power transmission from the plant to the load center inland. Because this power transmission requires submarine cables, there is a need to use high-voltage direct current (HVDC) transmission, which is economical for distances greater than 50 km. In the concept presented here, the onshore substation was operated at 60 Hz synced with the grid, and the offshore substation was operated at variable frequency and voltage, allowing the WPP to be operated at constant volt/hertz. In this paper, a variable frequency at rated volt/hertz operation was applied to a Type 3 doubly fed induction generator (DFIG) wind turbine generator. The size of the power converter at the turbine can be significantly reduced from 30% of the rated power output in a conventional Type 3 turbine to 5% of the rated power. The DFIG allows each turbine to vary its operating speed with respect to the other turbines. Thus, small wind diversity within the WPP can be accommodated by the DFIG, and the collector system frequency can be controlled by HVDC to follow large variations in average wind speed.**

***Index Terms*—wind turbine generator, variable speed, induction generator, HVDC, HVAC, renewable energy**

I. Introduction

The use of high-voltage direct current voltage-sourced converters (HVDC-VSC) has been proposed for offshore power systems, including renewable energy resources [1]–[3], because these systems become more economical than alternating current systems for transmission over distances greater than 50 km in an offshore environment. Although the dynamics of the high-voltage direct current (HVDC) itself are important [4], [5], we focused our investigation on the wind turbine and plant operation. The use of HVDC confers another advantage in that it is able to operate at variable frequency: several studies have proposed different control algorithms with the wind power plant (WPP) interconnected with HVDC-VSC [6], [7].

Figure **1** illustrates the layout diagram of the offshore WPP. In our proposed control strategy, the HVDC connecting the offshore WPP substation was operated at variable frequency at constant volt/hertz, and the onshore substation was operated at 60 Hz connected to the grid inland. The collector system frequency and voltage followed the average wind speed. In previous work [8], we reported on constant volt/hertz operation of fixed-speed turbines; in this paper, we concentrate on Type 3 doubly fed induction generator (DFIG) turbines. At rated frequency, the collector system voltage level was 34.5 kV, 60 Hz. At the turbine level, the pad mounted transformer converted the voltage to the generator voltage level, for example, 4160 V, 60 Hz at rated frequency. The operating frequency and the voltage at the collector system changed, but the ratio of the voltage to the frequency was constant. In this paper, the performance of DFIG at rated volt/hertz operation and the size of the power converter needed for rated volt/hertz operation is explored in comparison to conventional DFIGs operated at 60 Hz. Results from dynamic simulations performed to illustrate the control algorithms proposed for HVDC, electrical generator and power converter, and aerodynamic controls are shown.

In this analysis, we assumed that the wind speed was relatively uniform over an offshore wind plant, compared to an onshore plant, because of elimination of surface roughness and terrain effects. Wake may affect the validity of this assumption, particularly when the wind is directed along the turbine rows. Observed power losses due solely to wake can be up to 10% for closely spaced wind plants [9]. In [10], the authors presented an analysis of variable frequency (though not constant volt/hertz) offshore plant operation and included a discussion of wake effects as well. In our analysis, we considered that the average wind speed measurements had already incorporated the wake-linked reductions. Wake effects may also increase the diversity of wind speed within the plant, but the 5% power converter discussed here is able to accommodate the 10% speed variation between turbines because of wake effects.

Because of the decoupling of the plant from the grid by the HVDC link, the HVDC grid side converter assumed the responsibilities of ensuring that low-voltage and fault ride-through criteria were met. Fault and low-voltage operation is not examined in this paper.

In this paper, the following sequence occurs. In section II, the doubly fed induction generator is explored based on steady state characteristics, and the size of the power converter needed for rated volt/hertz operation is explored in comparison to conventional DFIG operated at 60 Hz. Section III describes the dynamic simulation we performed to illustrate the control algorithms proposed for HVDC, electrical generator and power converter, and aerodynamic controls.

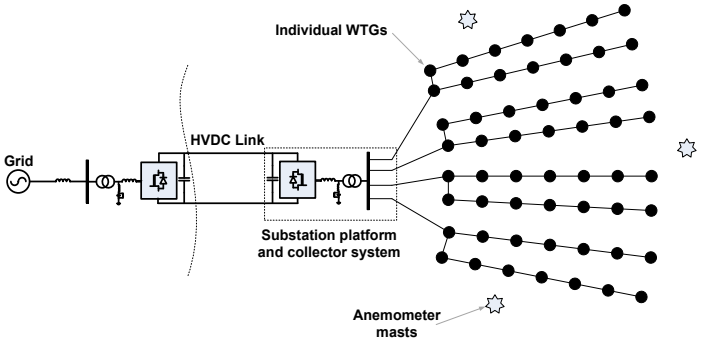

Figure 1. **Offshore WPP connected via HVDC to the grid**

II. Type III Wind Turbine—Doubly Fed Induction Generator with a Partial Rating Power Converter

Recently, the use of wound rotor induction machines has been revived in the form of an induction generator for wind turbine applications. With the power converter connected to the rotor winding, the induction generator can be operated at variable speed at partial load. A physical connection of the DFIG system is shown in Figure 2 below.

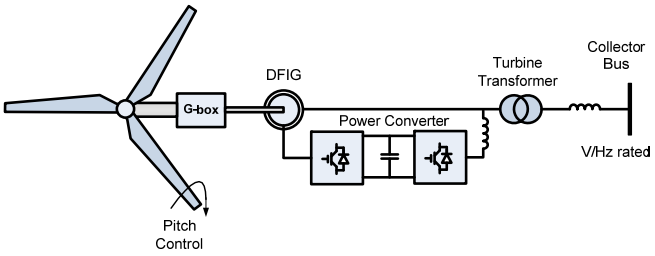

Figure 2. Physical connection diagram of a DFIG wind turbine generator

A. Basic Equations

From the equivalent circuit shown in Figure 3, we derived the equations to determine the size of power converter needed.

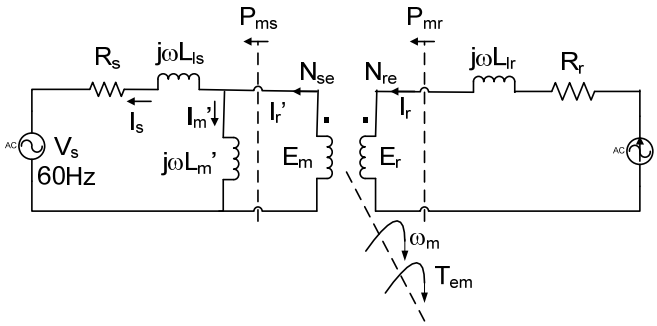

Figure 3. Per-phase equivalent circuit of the induction generator

From the equivalent circuit, the induced rotor emf E_r is proportional to the winding ratio and to the rotor frequency. In a locked rotor condition (slip=1), the stator-to-rotor winding relationship is similar to a transformer. As the slip gets smaller, the rotor voltage decreases. The relationship to the stator emf E_s can be written as

$$\frac{\boldsymbol{E_{mr}}}{\boldsymbol{E_{ms}}} = \frac{\boldsymbol{sN_{re}}}{\boldsymbol{N_{se}}}\boldsymbol{e^{i\theta_e}} \quad [1]$$

The current ratio is not affected by the rotor frequency and can be written as

$$\frac{\boldsymbol{I_r}}{\boldsymbol{I_s}} = \frac{\boldsymbol{N_{se}}}{\boldsymbol{N_{re}}}\boldsymbol{e^{i\theta_e}} \quad [2]$$

The ratio of the actual rotor impedance to the stator referred rotor impedance is

$$\frac{\boldsymbol{Z_r}}{\boldsymbol{Z_{r'}}} = \boldsymbol{s}\left[\frac{\boldsymbol{N_{se}}}{\boldsymbol{N_{re}}}\right]^2 \quad [3]$$

The useful active power at the stator side can be computed as

$$\boldsymbol{P_{ms}} = \mathrm{Re}[\boldsymbol{I_{ms}E_{ms}^*}] \quad [4]$$

The real power at the rotor side can be computed as

$$\boldsymbol{P_{mr}} = \mathrm{Re}[\boldsymbol{I_{mr}E_{mr}^*}] \quad [5]$$

By substitution, we can get the following equation

$$\boldsymbol{P_{mr}} = \mathrm{Re}[\boldsymbol{sI_{ms}E_{ms}^*}] \quad [6]$$

Or

$$\boldsymbol{P_{mr}} = \boldsymbol{s}\,\boldsymbol{P_{ms}} \quad [7]$$

Of the total air gap power of the generator, only a small fraction is dissipated in the rotor circuits. The mechanical power that is driven by the wind turbine is

$$\boldsymbol{P_{mechhhhh}} = (\boldsymbol{P_{ms}} - \boldsymbol{P_{mr}}) = (\boldsymbol{1} - \boldsymbol{s})\boldsymbol{P_{ms}} \quad [8]$$

Thus, mechanical/aerodynamic power generated by the wind turbine is converted into electrical power with the majority of the power delivered to the grid via the stator winding and a fraction of it delivered via the rotor output power. For example, assume the turn ratio of the stator-to-rotor winding relationship is one. The DFIG is to be operated at $\pm$ 30% slip. The power converter to be used must have about 30% rated voltage and 100% rated current. The implication is that to use a DFIG in variable speed with slip variation between -30% to +30%, the size of the power converter is about 30% of the rated power of the induction generator.

B. Operation at Rated Volt/Hertz

From the equivalent circuit shown in Figure 3 and the equations presented in the previous section, the size of the power converter is based on the designed slip range, the effective turn ratio, and the rated output power.

If we had operated the collector system in a variable frequency mode while maintaining rated volt/hertz, the operating magnetizing flux would have been constant at its rated value. The voltage rating of the power converter can be computed from its rated frequency and the maximum operating slip. For example, consider a DFIG designed to operate at $\pm$5% slip variation with rated voltage at 4160 V, 60 Hz. The voltage rating of the power converter would be 208V operating at 60 Hz (1.0 p.u. rated frequency).

If we connected the DFIG to a variable frequency source at rated volt/hertz and the frequency of the collector system was varied down to 30Hz (0.5 p.u.), the voltage at the rotor E_{mr} at 5% slip condition would be 5% x 0.5 x 4160 V = 104 V. Then, if the power converter was rated at 208 V, the operating slip range at 30 Hz could be increased to $\pm$10% slip without exceeding the rated voltage (10% x 0.5 x 4160 V = 208 V) of the power converter at 60 Hz. As shown in Figure 4, there was additional headroom to increase the range of operating slip at rated volt/hertz operation in the low operating frequency (corresponding to low wind speed).

To illustrate the concept, a typical DFIG was operated both at conventional operation (constant frequency at 60 Hz) and at variable frequency at constant rated volt/hertz. The DFIG was operated at unity power factor at its stator winding output.

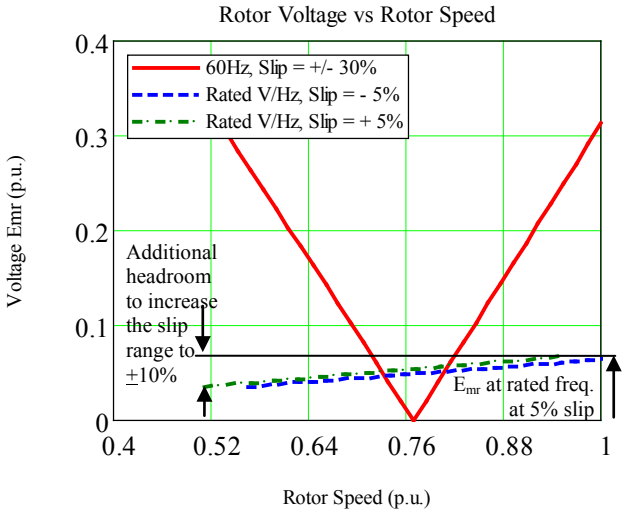

Figure 4. Voltage Emr variation at the rotor winding

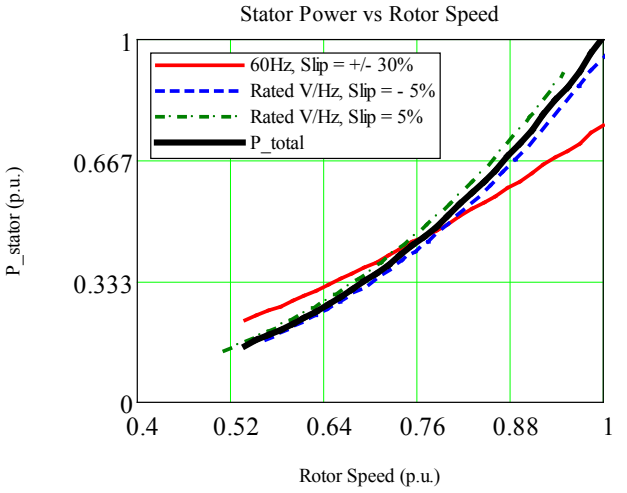

Figure 5. Stator output power versus rotor speed

In Figure 5, a typical output power of the stator winding was plotted against rotational speed. The first curve (solid red line) is a conventional doubly fed induction generator operated at 60Hz with the rotor slip operated within ± 30% slips. The next two curves (dashed blue and dot-dashed green lines) are the converter (rotor winding) output power with the operation of the wind turbine generator (WTG) kept at rated volt/hertz with the slip kept constant at -5% and +5% respectively. The last curve is the total output power from the stator winding and from the rotor winding, shown as a solid thick black line with the WTG operated at maximum performance coefficient (C_{p_max}). There were several observations worth noting:

- The difference between the total output power (solid black line) and the stator output power was the output power delivered by the rotor winding via the power converter.
- The size of the power delivered via the power converter was proportional to the slip and the output stator power.
- The total output power of the WTG crossed the output power of the stator winding, indicating that below synchronous rotor speed, the output of the power converter flows into the rotor winding, crossing the air gap, and into the grid via the stator winding. Above synchronous speed, the output of the power converter flows out of the rotor winding and is delivered to the grid via the power converter.
- Operating at lower slips (5%), the proportion of the output power from the rotor winding at rated speed was larger than the conventional operation with maximum operating slip of 30%.
- The size of the power delivered via the converter was determined by the maximum operating slip allowed by the operating design.

C. Power Converter Sizing

As shown in Figure 6, the ratio of the output power from the rotor to the output power from the stator was proportional to the operating slip. In the case of conventional operation of DFIG, the ratio of the power showed a linear line, as expected. On the other hand, if we maintained the operating slip constant, the rated volt/hertz operation showed a constant ratio (e.g., +5% or -5%).

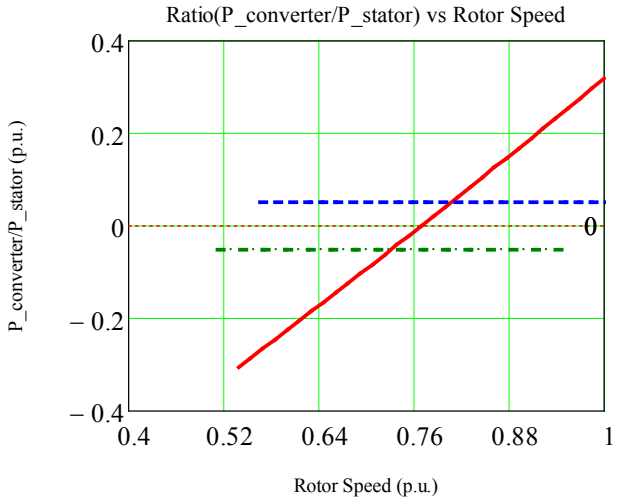

Figure 6. Ratio of P_rotor/P_stator versus rotor speed

Ideally, it is expected that all WTGs will operate at a very narrow slip. Although wind speed in an offshore WPP is generally consistent, there is a small diversity among wind speed from turbine to turbine; thus, realistically, the operating slips of individual turbines may vary between -5% and 5%. The power converter sized at 5% of the rated stator power would be sufficient to cover the diversity range in an offshore WPP.

In Figure 7, the output of the power converter is shown as a function of the rotor speed. The positive sign indicates that the output power flows out of the rotor winding; the negative sign indicates that the output power flows into the rotor winding. Note that in an ideal situation, when the wind speed is totally

uniform within the WPP, the rotor power of the WTG is practically zero, with the operating frequency matching the variation of the wind speed.

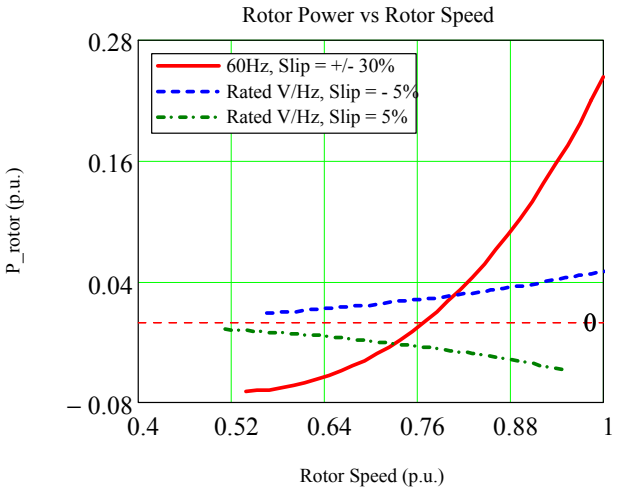

Figure 7. Rotor power output versus rotor speed

In Figure 7, the rating can be computed from the apparent power of the power converter. As shown, the apparent power is determined by the allowable operating slips. It indicates that with rated volt/hertz operation in an offshore WPP with uniform wind speed, we can size the power converter at lower rating, i.e., 5% instead of 30%, as in the conventional operation. (The frequency is fixed at 60 Hz.)

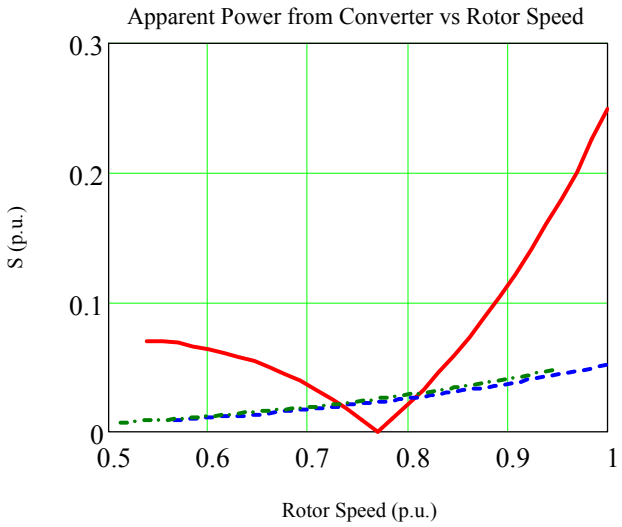

Figure 8. Power converter rating as a function of rotor speeds

D. Control Algorithm

1) HVDC Control and WTG Control Deployment

From the control diagram shown we showed that the sizing of the power converter is based on the designed slip range and operation at rated output power. The slip schedule and the rating of the power converter can be computed as

$$\boldsymbol{slip_{max}(f) = \frac{f_{rated}}{f} s_{max}} \quad [9]$$

The rating of the power converter can be sized at

$$\boldsymbol{MVA_{converter} = s_{max} MVA_{WTG}} \quad [10]$$

TABLE I
MAXIMUM OPERATING SLIP FOR DIFFERENT OPERATING FREQUENCIES USING RATED VOLT/HERTZ WITH 5% MAXIMUM SLIP AT RATED FREQUENCY

HVDC Operating Frequency	Maximum Operating Slip	Range of the Rotor Speed
1.0 p.u.	±5%	0.95 p.u.–1.05 p.u.
0.75 p.u.	±6.66%	0.70 p.u.–0.80 p.u.
0.50 p.u.	±10%	0.45 p.u.–0.55 p.u.
0.25 p.u.	±20%	0.20 p.u.–0.30 p.u.

If we operate the collector system in a variable frequency mode while maintaining rated volt/hertz, the operating magnetizing flux will be maintained constant at its rated value.

As shown in Figure 9, the WTG controller measured the operating frequency at the collector system. The frequency was used to compute the maximum allowable operating slip by using Table 1 presented above. The calculated maximum slip was then used to compute the maximum rotational speed at any operating frequency. When this maximum rotational speed was exceeded, the pitch controller adjusted the rotational speed to operate within allowable operating range.

The optimum operation of a wind turbine can be expressed as the target power P_{tgt} and written as

$$\boldsymbol{P_{tgt} = k_{wind} \omega_m^3} \quad [11]$$

where $k_{wind} = \frac{1}{2} \rho C_{pmax} \pi R_{blade}^5 \left(\frac{1}{TSR_{tgt}}\right)^3$

The tip speed ratio can be computed as

$$\boldsymbol{TSR = \frac{\omega_m R_{blade}}{V_{wind}}} \quad [12]$$

where TSR_{tgt} is the target tip speed ratio where $C_p = C_{pmax}$.

The tip speed ratio shown in Equation 12 has a specific value called TSR_{tgt} that corresponds to maximum aerodynamic efficiency C_{pmax}. TSR_{tgt} is a constant value approximately between 8 and 9 for a commercial turbine. Thus, by keeping the tip speed ratio or the ratio between rotational speed (or operating frequency) to the wind speed, we can keep the operation of the WTG at maximum aerodynamic efficiency C_{pmax}.

From Equation 11, we derived the equation of the output current for constant volt/hertz. Assuming a unity power factor operation at rated volt/hertz, the power equation can also be written as

$$\boldsymbol{P_{wtg} = 3 V_s I_s} \quad [13]$$

From Equation 11 and Equation 13, we derived the output current as

$$\boldsymbol{I_s = k_I \omega_m^2} \quad [14]$$

where $k_I = \frac{K_{wind} P}{6 V_{S-rated}}$ (Note: P here denotes the number of poles.)

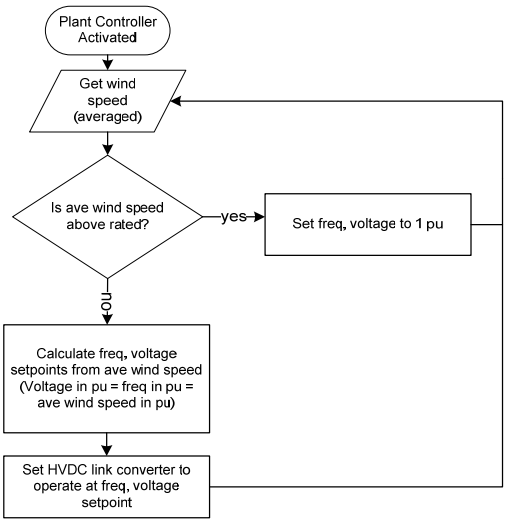

a) Plant level control flowchart

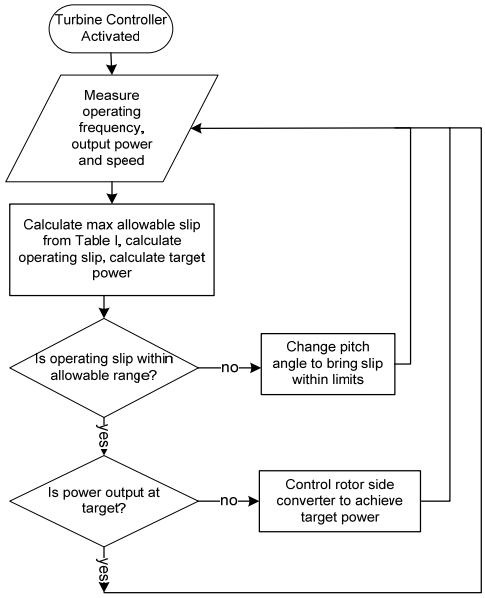

b) Turbine level control flowchart

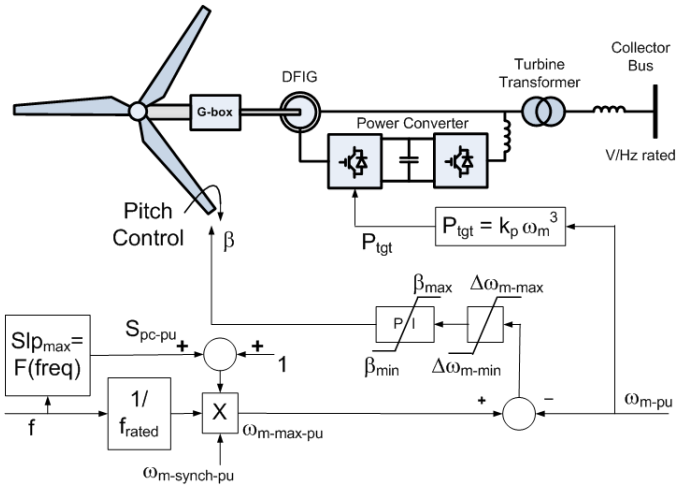

c) Turbine level control block diagram

Figure 9. Control implementation

The torque can be expressed by modifying Equation 11 as follows

$$T_{tgt} = k_{wind}\omega_m^2 \quad [15]$$

From Equation 14 and Equation 15, we can see that the output current of the WTG is proportional to the electromagnetic torque of the generator; thus, the stator current is a convenient way to observe the electromagnetic torque. The power converter will always be controlled to follow the target power based on the operating speed. With this control algorithm, the aerodynamic output power will be optimized and the turbine will be operated in the C_{pmax} operating mode. More detail derivation of target power can be found in many literatures (e.g., [1]–[5]).

Consider the operating condition of a DFIG connected to a grid of 60 Hz when the rotor winding is connected to a variable frequency source. The operating slip varies from -0.25 p.u. to +0.25 p.u. The rotor speed of the low speed shaft reaches synchronous speed of the generator at 0.8p.u. (shownas Point A in Figure 10. The actual generator's synchronous speed is 1,200 rpm (6 pole, 60 Hz). Thus, the generator is operated between 900 rpm and 1500 rpm, which correspondsto 0.6 p.u. to 1.0 p.u. at the low speed shaft. The power converter needed is 25% of the rated power of the generator. The operation of the WTG is depicted by the area covered by horizontal stripes.

Consider the operating condition of a DFIG connected to a grid of 60 Hz when the rotor winding is connected to a power converter. The operating slip varies from -0.05 p.u. to +0.05 p.u. The operation of the WTG is depicted by the area covered by gray shade. The synchronous speed is shown as Point B in Figure 10 (rotor speed=0.95 p.u.). The operation of this WTG is much narrower than the one with 25% rating power converter. However, the power converter for this operation is sized at only about 5% of the full rating of the generator. The operation of the WTG is depicted by the area covered by vertical stripes, with operating speed ranges from 0.9 p.u. to 1.0 p.u.

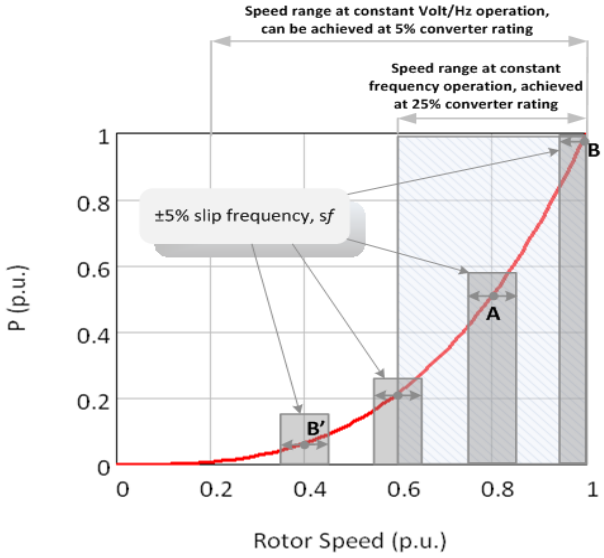

Figure 10. Variable speed operation at constant 60 Hz grid and variable speed operation at variable grid frequency.

If the collector system was connected to a substation with an HVDC transmitting power from an offshore WPP inland, the operating frequency of the collector system would be adjustable. As shown in Figure 1, the HVDC was operated at rated volt/hertz, allowing the collector system voltage and frequency to vary with time. The operation of the WTG is depicted by the area covered by gray shade, with operating speed ranges between 0.9 p.u. and 1.0 p.u. Note that the area can be moved along the speed axis by changing the operating frequency of the HVDC at the offshore substation.

TABLE II
COMPARISON BETWEEN 60 HZ OPERATION AND HVDC OPERATED AT RATED VOLT/HERTZ

	60 Hz Operation	HVDC at rated V/Hz
Rotor Speed	0.6p.u.–1.0p.u.	0.2p.u.–1.0p.u.
Power Converter	25%	5%

The operation of the WTG is depicted by the moving area covered by vertical stripes, with the operating speed varying within 5% with respect to the operating synchronous speed. The synchronous speed of the WTG changes with the HVDC operating frequency. For example, the synchronous speed is shown as Point B in Figure 10. When the HVDC frequency is moved to 0.4 p.u., the operating maximum slip variation is $\pm$ 7.5%, and the operating rotor speed ranges between 0.325 p.u. and 0.475 p.u. Thus, as summarized in Table II, with the variable frequency collector system, a wider speed range of operation can be achieved with a small size power converter. The converter size is very important, especially for a large wind turbine in offshore wind power deployment.

2) Pitch Control Activation

The pitch controller must be deployed to shed some of the aerodynamic power, thus limiting the slip and consequently keeping the stator current from exceeding the rated stator current. If the pitch angle is not changed, eventually the overload current may develop enough heat to cause insulation failure and short-circuit the stator winding. In addition, the power converter switches have very firm limits on current conduction capability.

If a wind turbine received a significantly higher wind speed than the $V_{W\text{-}ave}$ used to determine the frequency and voltage, it would generate a higher output power and the output current could exceed the rated current. To protect an individual wind turbine from operating at an overload condition, pitch needs to be controlled to stay below its rated output current.

III. DYNAMIC SIMULATIONS

A. HVDC Control Implementation

A dynamic simulation of the HVDC control was implemented at the offshore substation. The dynamic simulations shown examined the behavior of one wind turbine under volt/hertz control; however, if wind diversity within the plant was assumed to be small, this turbine's behavior would have been representative of the plant's behavior. In Figure 11, the frequency of the collector system varied based on the average wind speed measured. This variation was computed based on Equation 12 presented above and illustrated in the control block diagram shown in Figure 9.

The frequency was controlled to follow the wind speed variation to achieve maximum C_p operation for the majority of the turbines within the WPP. Similarly, the operating voltage was computed based on the variation of the frequency to maintain constant and rated volt/hertz, so that all the transformers and generators operated around rated flux and avoided magnetic saturation. Note that the operating frequency was limited at its rated frequency, which corresponds to the rated wind speed. Above rated wind speed, the frequency was constant, and the rotor speed was limited to its rated speed by controlling the pitch angle of the blades, limiting aerodynamic power from the wind.

B. WTG Electrical Control Implementation

The DFIG was operated at constant reactive power. The output power of the DFIG was controlled to follow the target power based on the variation of the rotational speed. (Refer to Equation 11 to compute the target power P_{tgt} and the control diagram shown in Figure 9.) The output power and reactive power of the DFIG is shown in Figure 12. The real and reactive power output of the DFIG was controllable independently and instantaneously. The WTG was operated with a combination of implementing electrical control of the power converter and aerodynamic control (pitch actuator). The output current as described in Equation 14 and Equation 15 was proportional to the electromagnetic torque. By comparing Figure 13 and Figure 14, we observed the relationship between the output current and the electromagnetic torque.

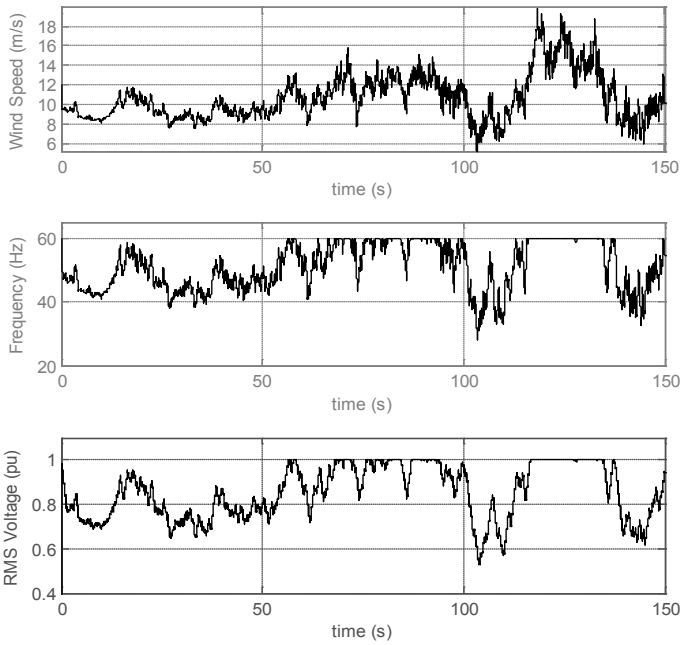

Figure 11. Variation of the wind speed and its corresponding frequency and voltage

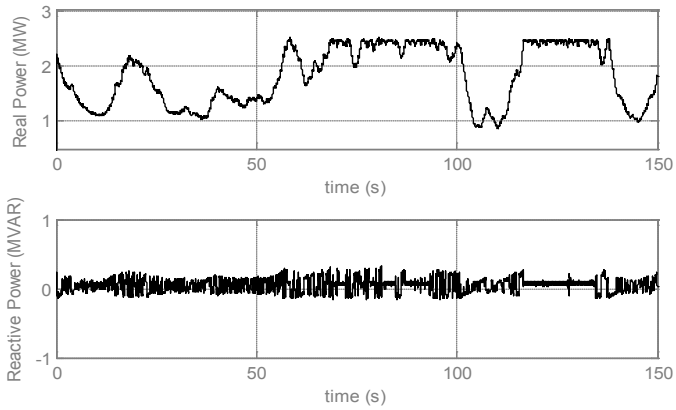

Figure 12. Real and reactive power output of the WTG

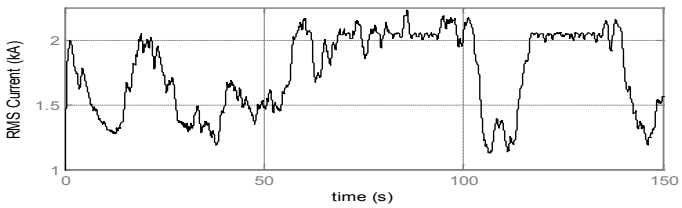

Figure 13. Output current of the WTG

C. WTG Aerodynamic Control Implementation

Figure 9 illustrates the aerodynamic control. The pitch angle was controlled to ensure that the rotor speed did not exceed the prescribed maximum operating slip (e.g., 5%); however, as described in Figure 4, there was headroom to double this maximum operating slip (to 10%) at half the rated speed.

Figure 13 shows that the pitch was successfully controlled to limit the rotational speed as obvious in the higher wind speed region, where the frequency of the collector system reached its limit, and the rotational speed was successfully limited by the aerodynamic control implemented via pitch controller.

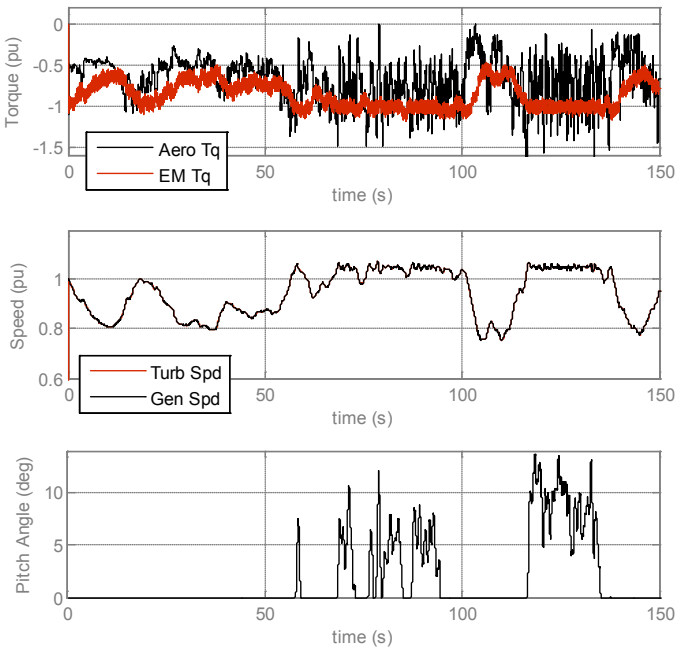

Figure 14. The torque, rotational speed, and pitch angle

D. Harmony Among the HVDC Control, Electrical WTG Control, and Aerodynamic WTG Control

The harmony among different controls of the entire WPP is illustrated in Figure 15. Consider the performance coefficient curve shown in Figure 15. In the lower wind speed region, the HVDC controlled the frequency to follow the wind speed average. The voltage output was also controlled so that the collector system connected to the HVDC at the onshore substation generated rated volt/hertz, ensuring that the electromagnetic fluxes within the WPP avoided saturation.

The power converter of the WTG ensured that the DFIG was at maximum operating C_p by following the target power expressed by Equation 11. As shown in Figure 15, in the first 70 s of the simulation, the operating C_p was at its maximum. As the wind speed increased, the maximum operating frequency was reached and the HVDC control was frozen to maintain constant voltage and constant frequency corresponding to rated volt/hertz.

Because we could not control wind speed, the pitch controller was activated when the wind speed increased beyond its rated, thus avoiding a runaway situation. As shown in Figure 14 and Figure 15, the aerodynamic power was well maintained by the pitch controller by operating the WTG at a much lower aerodynamic efficiency (refer to the C_p between 70 s and 95 s and between 115 s and 135 s).

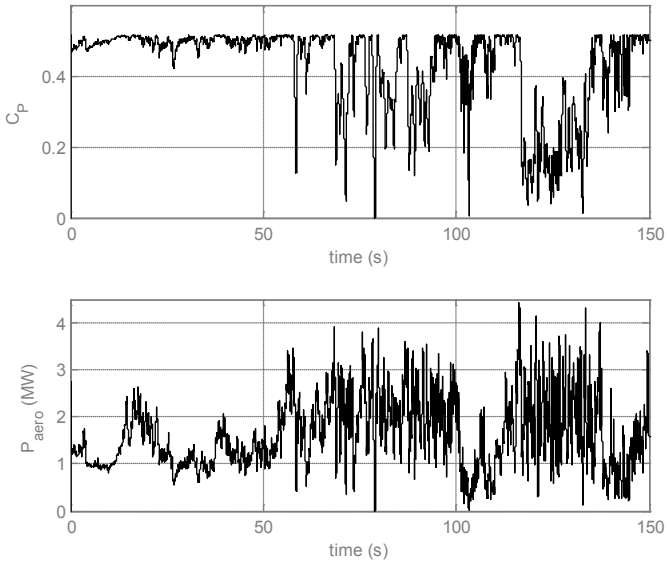

Figure 15. Performance coefficient C_p and aerodynamic power

IV. Conclusions

Rated volt/hertz operation for an offshore WPP takes advantage of the availability of the HVDC-VSC to vary the frequency and voltage at the collector system. This paper investigates Type 3 WTG (DFIG) operated under rated volt/hertz. With uniform wind speed in an offshore WPP, the size of the power converter at each WTG can be minimized by matching the frequency of the collector system to the wind speed average. The use of a small power converter at 5% of its rated power proved to be sufficient for the wind speeds under consideration with possible additional slip range in lower wind

speed. The combination of controllers (HVDC, power converter, and pitch control) makes it possible to smooth out the output during transients, thus allowing a better mechanical compliance between the wind turbine and the generator while maintaining the C_{pmax} operation up to rated wind speeds.

V. Future Plan

At the conclusion of this study, we plan to test the concept at the National Renewable Energy Laboratory's Energy System Integration Facility using small-scale units and Real Time Digital Simulator system with hardware in the loop. Eventually, a field test is necessary to verify the control systems at our test site (National Wind Technology Center) using our 9MVA Grid Control Simulator. In future work, we will quantify the benefit of implementing this concept from the energy yield point of view, and also study the impact on WPP dynamics of various control schemes.

VI. Acknowledgment

This work was supported by the U.S. Department of Energy under Contract No. DE-AC36-08-GO28308 with the National Renewable Energy Laboratory.

VII. References

[1] Bodin, A. "HVDC Light—A Preferable Power Transmission System for Renewable Energies." *Proceedings of the 2011 Third International Youth Conference on Energetics*; July 7–9, 2011, Leiria, Portugal.

[2] Rui, O; Thon, J.; Sand, H.; Waalman, J.G.; Bjerknes, O.J.; and Karijord, K. "Design and Operation of an Offshore Node Connected to Wind Parks, Oil Platforms as Well as a Multiterminal HVDC Grid." *Ninth International Workshop on Large-Scale Integration of Wind Power into Power Systems as well as on Transmission Networks for Offshore Wind Power Plants*, Oct. 18-19, 2010, Québec City, Canada.

[3] MacLeod, N.M.; Barker, C.D.; and Kirby, N.M. "Connection of Renewable Energy Sources through Grid Constraint Points using HVDC Power Transmission Systems." *2010 IEEE PES Transmission and Distribution Conference and Exposition*, April 19–22, New Orleans, Louisiana.

[4] Feltes, C.; Wrede, H.; Koch, F.W.; and Erlich, I. "Enhanced Fault Ride-Through Method for Wind Farms Connected to the Grid Through VSC-Based HVDC Transmission." IEEE Transactions on Power Systems (24: 3), Aug. 2009.

[5] Feltes, C., and Erlich, I. "Variable Frequency Operation of DFIG-Based Wind Farms Connected to the Grid Through VSC-HVDC Link." *IEEE Power Engineering Society General Meeting*, June 24–28, 2007, Tampa, Florida.

[6] Trilla, L.; Gomis-Bellmunt, O.; Junyent-Ferre, A.; and Sudria-Andreu, A. "Analysis of Total Power Extracted with Common Converter Wind Farm Topology." *XIX International Conference on Electrical Machines*, Sept. 6–8, 2010, Rome, Italy.

[7] Jovcic, D. "Interconnecting Offshore Wind Farms Using Multiterminal VSC-based HVDC." *IEEE Power Engineering Society General Meeting*, June 18–22, 2006, Montreal, Quebec, Canada.

[8] Gevorgian, V.; Singh, M.; and Muljadi, E. "Variable Frequency Operations of an Offshore Wind Power Plant with HVDC-VSC." Preprint. Prepared for IEEE Power Engineering Society General Meeting, July 22–26, 2012, San Diego, California: Available at http://www.nrel.gov.

[9] Barthelmie, R.J.; Frandsen, S.T.; Nielsen, M.N.; Pryor, S.C.; Rethore, P.-E.; and Jørgensen, H.E. "Modeling and Measurements of Power Losses and Turbulence Intensity in Wind Turbine Wakes at Middelgrunden Offshore Wind Farm." *Wind Energy* (10: 6), 2007; pp. 1099-1824.

[10] de Prada Gil, M.; Gomis-Bellmunt, O.; Sumper, A.; and Bergas-Jané, J. "Analysis of a Multi-Turbine Offshore Wind Farm Connected to a Single Large Power Converter Operated with Variable Frequency." *Energy* (36: 5), May 2011; pp. 3272–3281: http://www.sciencedirect.com/science/article/pii/S0360544211001769.

VIII. Biographies

Eduard Muljadi (M'82, SM'94, F'10) received his Ph.D. in electrical engineering from the University of Wisconsin at Madison. From 1988 to 1992, he taught at California State University at Fresno. In June 1992, he joined the National Renewable Energy Laboratory in Golden, Colorado. His current research interests are in the fields of electric machines, power electronics, and power systems in general with an emphasis on renewable energy applications. He is member of Eta Kappa Nu and Sigma Xi, a Fellow of the Institute of Electrical and Electronics Engineers (IEEE), and an editor of the IEEE Transactions on Energy Conversion. He is involved in the activities of the IEEE Industry Application Society (IAS), Power Electronics Society, and Power and Energy Society (PES). He is currently a member of various committees of the IAS, and a member of the Working Group on Renewable Technologies and the Task Force on Dynamic Performance of Wind Power Generation, both of the PES. He holds two patents in power conversion for renewable energy.

Mohit Singh (M'11) received his M.S. and Ph.D. in electrical engineering from the University of Texas at Austin in 2007 and 2011 respectively. His research is focused on dynamic modeling of wind turbine generators. Dr. Singh is currently working at the National Renewable Energy Laboratory (NREL) in Golden, Colorado, USA, as a post-doctoral researcher in transmission and grid integration of renewable energy. His current interests include modeling and testing of various applications of wind turbine generators and other renewable energy resources. He is a member of the IEEE. He is involved in the activities of the IEEE Power and Energy Society (PES).

Vahan Gevorgian (M'97) graduated from the Yerevan Polytechnic Institute in Armenia in 1986. During his studies, he concentrated on electrical machines. His thesis research dealt with doubly fed induction generators for stand-alone power systems. He obtained his Ph.D. in electrical engineering from the State Engineering University of Armenia in 1993. His dissertation was devoted to modeling electrical transients in large wind turbine generators.

Dr. Gevorgian is a research engineer at the National Wind Technology Center of the National Renewable Energy Laboratory in Golden, Colorado. His current research interests include modeling and testing various applications of small wind turbine–based power systems.